Microelectronic Engineering 263 (2022) 111841

Contents lists available at ScienceDirect

Microelectronic Engineering

journal homepage: www.elsevier.com/locate/mee

A novel room temperature SO_2 gas sensor based on TiO_2/rGO buried-gate FET

Simei Zeng, Ying Zhang, Yang Zhang, Yuning Li, Chenggang Tang, Ke Li, Jingye Sun, Tao Deng *

School of Electronic and Information Engineering, Beijing Jiaotong University, Beijing 100044, China

ARTICLE INFO

Keywords:
Buried-gate FET
TiO_2
Reduced graphene oxide
Interdigitated electrode
SO_2 gas sensors

ABSTRACT

Gas sensors are able to detect the type and concentration of flammable, explosive, toxic gases (e.g. NO_2, SO_2, NH_3), showing wide applications in petroleum, chemical, medical, transportation and safety protections in the domestic and industrial environment. Currently, the SO_2 gas sensors are mainly based on metal oxide semiconductors. However, its operating temperature is generally much higher than room temperature, and the operation at higher temperature often requires complex circuits and high power consumption. A novel room temperature (RT) SO_2 gas sensor based on buried-gate field effect transistor (FET) and interdigitated electrode structure with titanium dioxide (TiO_2) nanoparticles and reduced graphene oxide (rGO) composite materials as gas-sensitive layer, has been fabricated and demonstrated in this paper. The TiO_2/rGO FET sensor shows a relative high responsivity (3.46%) to 20 part per million (ppm) SO_2 gas, under a source-drain voltage of 2 V and a zero gate voltage. Experimental results have shown that the responsivity and response-recovery time of the sensor could be controlled by the source-drain voltage. This paper demonstrates the feasibility of TiO_2/rGO nanocomposite as a gas-sensing material for high-performance SO_2 gas sensors. In addition, this approach would provide a feasible way for the realization of miniaturized, integrated and high-performance SO_2 gas sensors.

1. Introduction

Nowadays, the environmental problems caused by the rapid economic growth have become the focus of people's attention. The World Health Organization reported that 4.2 million people die every year due to air pollution caused by nitrogen dioxide (NO_2), sulfur dioxide (SO_2), ammonia (NH_3) and other harmful gases. As one of the typical air pollutants, SO_2 is generally generated by burning fossil fuels in power plants, transportation services and other industrial facilities, and is consider as a toxic gas that harms the environment and human health [1]. On the one hand, SO_2 is easily dissolved in cloud droplets, forming acid rain and affecting the natural balance of rivers, lakes and soils, which would cause the damage to wildlife and vegetation. On the other hand, SO_2 will harm human's health. The long-term and short-term thresholds for human exposure to SO_2 gas are 5 ppm and 2 ppm, respectively [2,3]. Beyond these thresholds, human's cerebral cortex and respiratory system functions will be impaired, resulting in a variety of diseases, and even death in severe cases [4,5]. Therefore, qualitative and quantitative analysis for SO_2 gas detections are urgent problems to be solved in atmospheric environmental protection. The SO_2 gas sensors can detect the concentration of SO_2 gas and output the gas information in a form of electrical signals. According to different working mechanisms, they are mainly divided into electrochemical SO_2 gas sensors, surface acoustic wave SO_2 gas sensors, optical SO_2 gas sensors and metal oxide semiconductor (MOS) SO_2 gas sensors [6]. Among them, MOS SO_2 gas sensors are widely used in the market, showing the merits of small size, low manufacturing cost and simple preparation process. Meanwhile, they also have the advantages of high sensitivity, and fast response and recovery time [7]. Metal oxide semiconductors employed SnO_2 [8], WO_3 [9], ZnO [10], TiO_2 [11], etc., as SO_2 gas-sensitive materials. However, this kind of sensors usually work under high-temperature environment and requires high power consumption, which affect the integration and long-term stability of the sensors. Hence, it is necessary to seek for new materials to be combined with MOSs and design suitable sensor structures to reduce the working temperature of SO_2 gas sensors.

In recent years, graphene and its derivatives, such as original graphene, graphene oxide (GO) and reduced graphene oxide (rGO), have

* Corresponding author.
E-mail address: dengtao@bjtu.edu.cn (T. Deng).

https://doi.org/10.1016/j.mee.2022.111841
Received 26 May 2022; Received in revised form 28 June 2022; Accepted 3 July 2022
Available online 8 July 2022

been characterized by good thermal stability, super conductivity, high carrier mobility at room temperature, large specific surface area and low electrical noise. It is considered as a promising room-temperature gas sensing material [12]. rGO is reduced from GO, containing many functional groups and defects [13]. As a derivative of graphene, rGO has the advantages of low cost, good thermal conductivity and hydrophilicity. Moreover, the oxygen functional groups and structural defects on its surface can be used as the active sites for gas adsorption. Compared with graphene, rGO is a p-type semiconductor. When the target detection gas is exposed to the rGO, the charge of rGO will be transferred to the gas molecule to become ions. The binding mode between the target gas molecule and rGO changes from van der Waals force to a covalent bond [14]. In addition, rGO has a large number of gas auction sites. For example, oxygen-containing functional groups, defects and hybrid carbon atoms in rGO would greatly improve the contact between target gas molecules and rGO, and enhance the response performance of gas sensors [15]. Meanwhile, the unique oxygen-containing functional groups (such as carboxyl, hydroxyl groups) and the unique lamellar structure of rGO are conducive to the formation of composite material sensing films [16]. Last but not least, the application of rGO in gas sensing can effectively reduce the working temperature, and provide the possibility of working at room temperature [17]. Many rGO composites (such as metal particles [16], metal oxides [18,19] or polymers [20]) are used to detect room-temperature target gases. In conclusion, combining MOSs with rGO will enable the SO_2 gas to be sensed at room temperature.

Immense amounts of research have proved that the combination of MOSs material with rGO could greatly reduce the operating temperature and improve the gas sensitivity of the sensors. Tyagi et al. prepared rGO-SnO_2 and MWCNT-SnO_2 by chemical methods [21]. The composites were respectively coated on the surface of Pt interdigital electrodes for the detection of SO_2 gas. Compared with the MWCNT-SnO_2 and bare SnO_2 sensors, the rGO-SnO_2 gas sensor shown a larger sensing response value and a relatively fast response and recovery times of 2.4 mins and 3.5 mins at low operating temperature of 60 °C. Li et al. compared the sensitivities of rGO-modified SnO_2 hollow nanofibers to SO_2 and NO_2 before and after UV excitation at room temperature [22]. It has been found that the responsivity and selectivity of the sensors could be improved by using appropriate intensity of UV light. However, this method has certain limitations for the development of portable sensors and increases the complexity of gas sensor preparation. Another method for preparing room temperature SO_2 gas sensors is to combine TiO_2 with rGO. As a semiconductor material with a wide bandgap (3.0–3.2 eV), TiO_2 has the advantages of low cost, excellent catalytic performance and room temperature operation. Zhang et al. synthesized TiO_2/rGO films by using layered self-assembly technology, which could be used for SO_2 detection at room temperature [23]. When the sensor was placed in SO_2 gas with various concentrations, the response of the sensor increased with the increase in gas concentration, but the response-recovery time became longer. Zhang et al. fabricated an SO_2 gas sensor based on MOFs-derived TiO_2/rGO nanocomposites [24]. The MOFs TiO_2/rGO nanocomposite sensor shows better performance than pure TiO_2 sensors in the SO_2 concentration range from 250 ppb to 20 ppm, with a 43% responsivity to 1 ppm SO_2 gas. However, the large size of the sensor does not meet the development needs of integration and miniaturization.

In this paper, a novel room temperature SO_2 gas sensor with interdigitated electrode structure was fabricated by decorating FETs with rGO and TiO_2 NPs. The gas sensing film dimension of the TiO_2/rGO FET was only 130 μm × 200 μm. The electrical properties of the sensor were measured and the results shown that the sensor exhibit typical bipolar properties and good ohmic contact between the TiO_2/rGO film and electrodes. Moreover, the interdigitated electrode structure had better electrical performance than the conventional electrode structure. And a responsivity as high as 3.47% was obtained when the sensor was exposed to SO_2 gas with a concentration of 20 ppm at room temperature. Experimental results shown that the response and recovery times of the sensor were 456 s and 134 s, respectively. In addition, the responsivity could be further improved by applying a small gate voltage or increasing the source-drain voltage. The sensitive SO_2 gas sensor working at room temperature shows great potential in petrochemical and other heavy pollution fields.

2. Material and methods

2.1. The fabrication process

The fabrication process for the TiO_2/rGO FET is shown in Fig. 1. Firstly, under the condition of 85 °C, the silicon wafer was rinsed with hydrogen and sulfuric acid solution (the ratio of H_2O_2:H_2SO_4 is 1:4) for 15 mins. Then, an aluminum (Al) sacrificial layer with a thickness of 50 nm was sputtered on the pre-cleaned silicon wafer by using the magnetron sputtering method. SiN_x double stress layers were grown on Al sacrificial layer by the PECVD film formation technique, where a tensile strain SiN_x layer with a thickness of 80 nm was grown at a frequency of 380 kHz, and a compression strain SiN_x layer with a thickness of 50 nm was grown at a frequency of 13.56 MHz. A chromium/gold (10 nm/50 nm) gate electrode was sputtered on top of SiN_x layers, followed by depositing a 50 nm SiO_2 dielectric layer. Then, the silicon wafer was lithographed with negative photoresist NR9-3000PY. Subsequently, chromium/gold (10 nm/50 nm) source and drain interdigital electrodes were sputtered on the SiO_2 layer by using the magnetron sputtering and stripping method.

The next step was to prepare TiO_2/rGO composite films. Firstly, 20 mL GO solution (0.5 mg/mL, XFNANO) was mixed with 20 mL deionized water, and the mixed solution was ultrasonic for 20–30 min at a high power of 700 W to obtain a well-dispersed GO solution with a concentration of 0.25 mg/mL. Then, 8 mg TiO_2 powder (99.3 wt%, XFNANO) was mixed with 40 mL ethanol and the TiO_2 was well dispersed by ultrasound for 2–3 h by a high-power ultrasonic machine of 800 W. Then TiO_2 solution with a concentration of 0.2 mg/mL was obtained. Finally, thin film-forming technology and a simple thermal reduction method were employed to prepare the sensing layer. 100 μL GO solution was drip-coated on the planar source and drain electrodes array and the sensor was dried in a drying oven at 60 °C for 30 min. This low-temperature heating process is conducive to enhance the contact between sensing material and electrodes. Then, a 6 μL TiO_2 dispersive droplet was dropped to the surface of the GO layer and the sensor was placed into a drying oven at 60 °C for 30 min to form the TiO_2/GO network structure. Finally, the sensor was annealed at 220 °C for 2–3 h to obtain a TiO_2/rGO sensing film with good conductivity. As a result, the TiO_2/rGO FET was prepared.

2.2. Characterization

The morphology of the TiO_2/rGO FET was characterized by using a scanning electron microscope (Gemini SEM 300). The transfer and output characteristic curves of the sensor were measured by a semiconductor parameter measuring instrument (Agilent B1500). The SO_2 gas detections were carried out in a closed container with controllable SO_2 concentration, as shown in Fig. 2. The gas bottles storing SO_2 gas and dry air were connected to the GC400 distributor, where the SO_2 gas was mixed with dry air to the desired concentration. One pipe filled with SO_2 gas was connected between the gas sensing chamber and the outlet of the GC400 distributor, and the other pipe was connected to the ventilation pipe to remove the excess gas and maintain the pressure in the chamber. The sensing chip was placed in the closed chamber. Before the gas detection, the chip was bonded onto a printed circuit board (PCB) with gold wires, connected to an Agilent Sourcemeter outside the container. The Sourcemeter would provide the bias voltage (V_{ds}) for the sensor. The response of the TiO_2/rGO FET was measured and the results were passed to a computer for further data processing. When conducting the gas sensing measurement, the current of the sensor was recorded primarily in the air state. Then the SO_2 gas with a concentration of 500

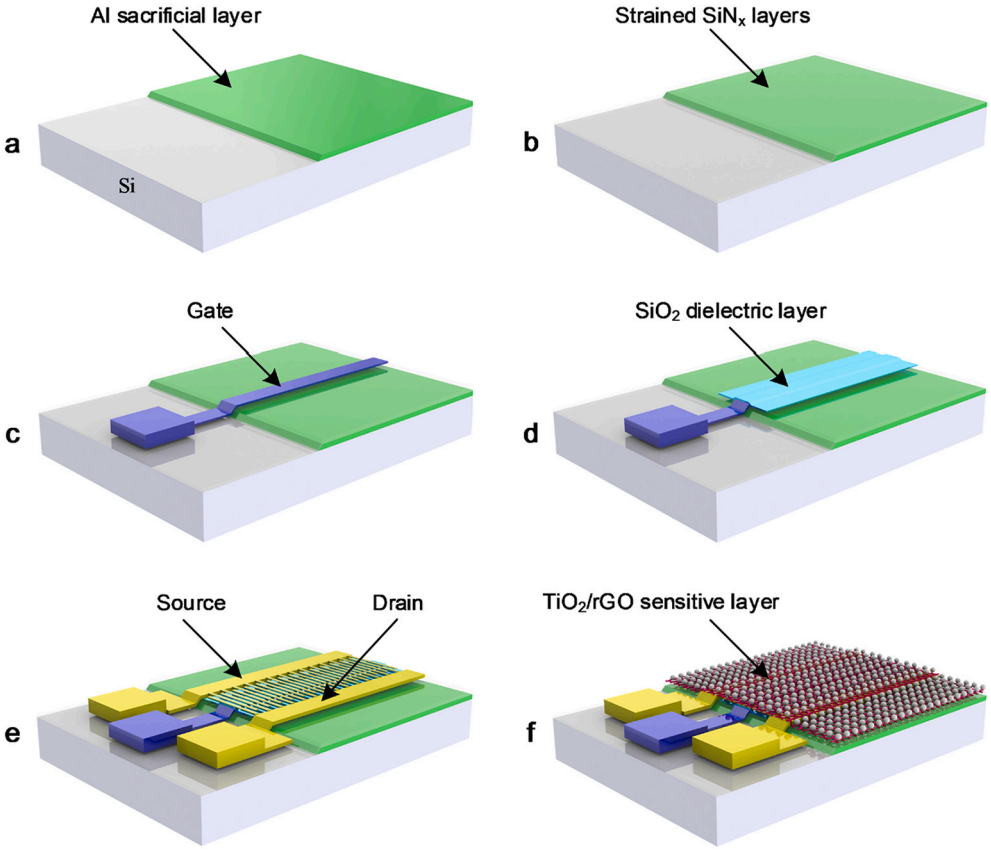

Fig. 1. The fabrication process for the TiO_2/rGO FET with interdigitated electrode structure. (a) Sputter an Al sacrificial layer. (b) Grow strained SiN_x layers. (c) Sputter the gate electrode. (d) Deposit a SiO_2 dielectric layer. (e) Sputter source and drain interdigital electrodes. (f) Form a TiO_2/rGO sensing layer.

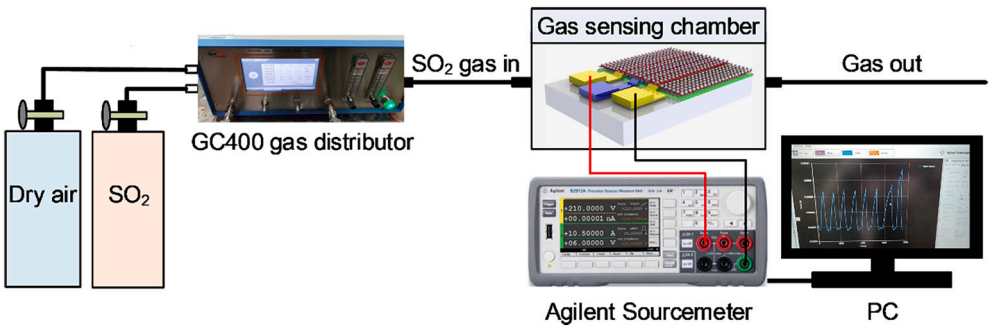

Fig. 2. The diagram of the SO_2 gas sensing system.

mL/min mixed by the GC400 gas distributor was pumped into the sensing chamber rapidly. It was observed at the computer that the current began to change when SO_2 gas was introduced. As the current was saturated, air was pumped into the chamber until the current returned to its initial value. The whole process was repeated several times and the experiment was carried out at room temperature.

3. Results and discussions

3.1. The gas sensing mechanisms of TiO_2/rGO composite film

The mechanisms of TiO_2/rGO composite film sensing SO_2 are as follows: The p-type rGO reacts with SO_2, causing the SO_2 molecules to become ions, where the chemical formula is give as $SO_2 + e^- \rightarrow SO_2^-$. The transfer of electrons from rGO to SO_2 molecules could result in a reduction in rGO resistance [17,25]. As the surface catalytic active center, TiO_2 nanoparticles can adsorb and dissociate O_2. Generally, oxygen adsorbents (O^- and O_2^-) are generated on the surface of TiO_2 at high temperatures. At room temperature, chemisorbed oxygen molecules can be ionized to O_2^- by capturing free electrons on the surface of TiO_2. When the TiO_2 surface is exposed to SO_2, the SO_2 molecules react with the O_2^- adsorbed on the TiO_2 surface and forms SO_3 through the reaction of $2SO_2 + O_2^- \rightarrow 2SO_3 + e^-$. Then the excess electrons are injected into the conduction band, thus increasing the electron concentration of TiO_2, and leading to the reduction in TiO_2 resistance [26].

In addition, heterojunctions are formed between p-type rGO and n-type TiO_2. The holes in rGO and electrons in TiO_2 will form a self-built electric field in the heterojunction region, and a depletion layer can be established when the Fermi level equilibrium is achieved. The adjustment of depletion layer width is attributed to the induction mechanism of SO_2 adsorption and desorption by TiO_2/rGO hybrid nanocomposites. When exposed to SO_2 gas molecules, the width of the depletion layer is

reduced, which will improve the conductivity of TiO_2/rGO hybrid nanocomposites and further enhance the gas-sensitive performance of the sensor.

3.2. Experimental results

Fig. 3a shows a 1 × 5 TiO_2/rGO FET sensor array, where two sensors share one electrode, indicating a feasible solution for mass production. As indicated in the figure, the dimension of the TiO_2/rGO film in a single sensor is 130 μm × 200 μm. From the enlarged image of the TiO_2/rGO FET sensor shown in Fig. 3b and c, the width between the source and drain interdigital electrodes is measured as 5 μm. Moreover, the TiO_2/rGO composite film and the interdigital electrodes form a closed loop, leading to an increase in the contact area between the film and the electrodes. Meanwhile, the shorter conductive channel speeds up the carrier transmission rate and improves the gas response. Fig. 3d shows the enlarged view of the conductive channel. It can be clearly seen that a large number of TiO_2 nanoparticles cluster together with particle sizes between 40 and 110 nm, due to the low power and short time ultrasonic treatment during the configuration process for the TiO_2 dispersion liquid.

The transfer characteristic curve reveals the ability of gate voltage V_{gs} to regulate the carrier within the sensing film. Fig. 4a shows the transfer characteristic curve of the TiO_2/rGO FET at $V_{ds} = 0.5$ V, and the interdigital electrode length of the sensor is 200 μm. As the voltage V_{gs} increases, the current I_{ds} of the sensor decreases and then increases, showing good bipolar characteristics. As can be seen from the transfer characteristic curve, the TiO_2/rGO sensor film shows p-type semiconductor characteristics and good gate control ability. Among them, the hole carriers in rGO conduct electricity and the Fermi level is close to the valence band. When V_{gs} is negative, a certain amount of positive charges are induced in the rGO material, which leads to the increase in hole concentration and the Fermi level moves to the valence band. When V_{gs} is positive, a certain amount of negative charges are induced in the rGO material and the concentration of hole decreases. Then the Fermi energy level begins to move towards the conduction band and the resistivity of the sensor decreases. When the resistivity reaches the minimum, the bias of the sensor reaches the Dirac point ($V_{gs} = 4$ V), and the hole concentration in the rGO material is equal to the electron concentration. Thereafter, as V_{gs} continues to increase, electron carriers are conducted in rGO, resulting in the increase in resistivity.

The output characteristic curve is used to judge the contact mode between the TiO_2/rGO layer and the electrodes. Fig. 4b shows the variation of I_{ds} against V_{ds} from 0 V to 0.5 V under the control of different gate voltages. It is obvious to see that I_{ds} increases linearly with the increase of V_{ds}, revealing a good ohmic contact between the TiO_2/rGO sensing film and the electrodes. In addition, the output characteristic curves of the sensor show different slopes under different V_{gs}, indicating that the gate voltage shows a good ability to regulate the source and drain current of the TiO_2/rGO FET.

The performance of the traditional GFET is evaluated by the speed of carrier migration rate in the conductive channel. Theoretically, the conductive channel is shorter, the carrier migration rate is faster [27]. The interdigitated electrode structure is designed in this paper, the distance between the source and drain electrode is narrow (5 μm). Therefore, the interdigitated electrode structure reduces the contact resistance between the electrodes and the sensing layer, so that the carrier transmission rate between the source and the drain electrode will be increased, and the electrical performance of the TiO_2/rGO FET could be greatly improved. Fig. 4c shows a comparison of the output characteristic curves of the TiO_2/rGO FET with conventional electrodes (14 μm) and interdigitated electrodes (5 μm) at a zero gate voltage. The results show that the proposed sensor has better electrical performance than the conventional electrode structure.

The response-recovery curve of the TiO_2/rGO FET exposed to SO_2 gas with a concentration of $C = 20$ ppm at room temperature is shown in Fig. 4d, under the condition of $V_{gs} = 0$ V and $V_{ds} = 2$ V. It is seen that I_{ds} begins to rise when SO_2 is introduced, since SO_2 acts as an electron

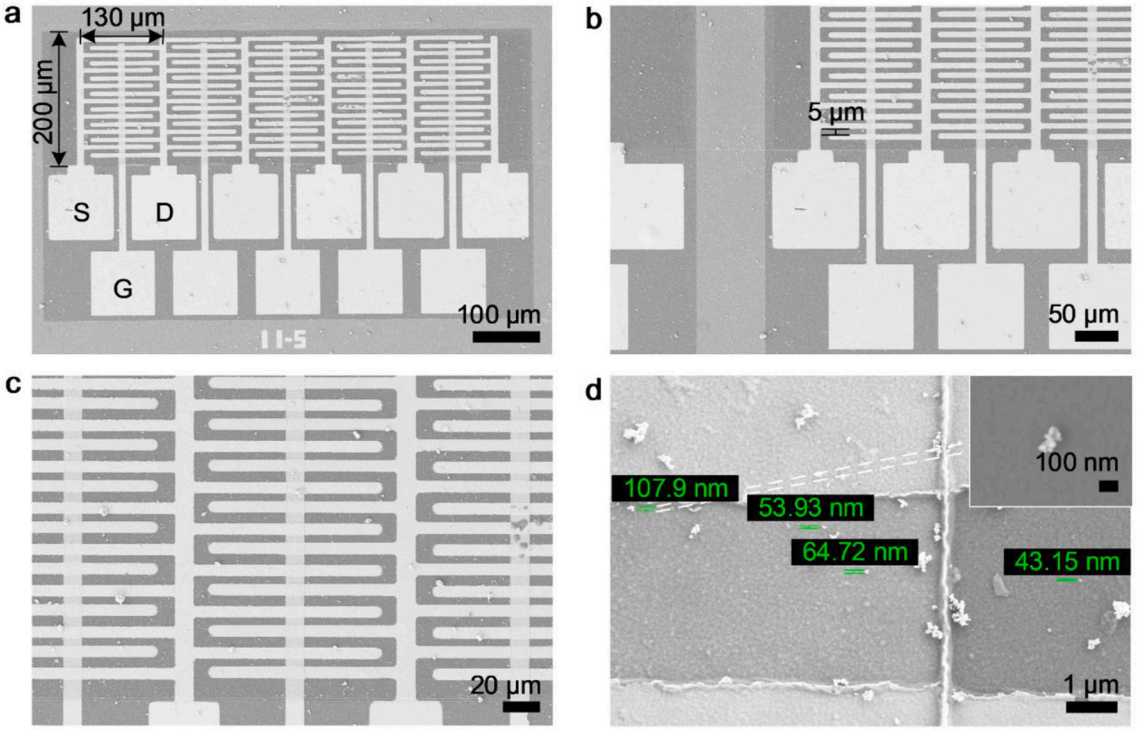

Fig. 3. SEM images of the TiO_2/rGO FETs with interdigitated electrode structure. (a) An array of the TiO_2/rGO FETs (1 × 5 sensors). (b) and (c) Zoomed-in view of the sensors (the width between the source and drain interdigital electrodes is 5 μm). (d) Zoomed-in view of the conductive channel (upper right is an enlarged image of the pointed part).

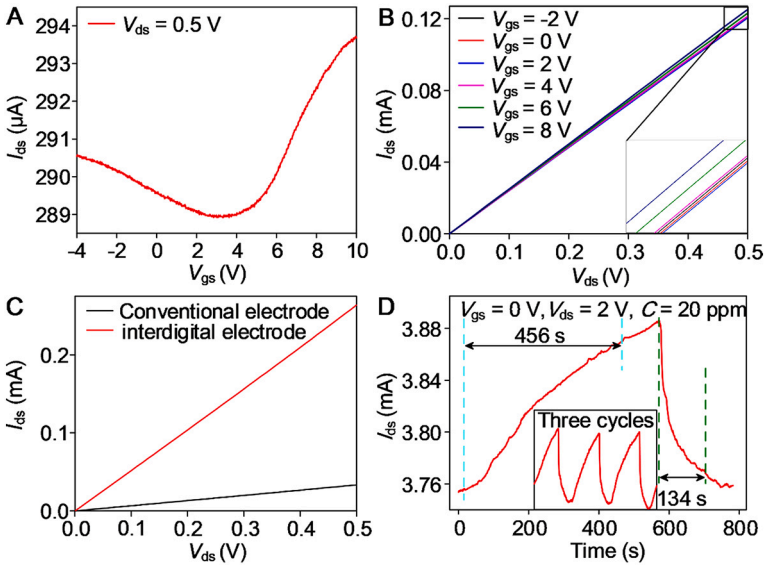

Fig. 4. (a) The transfer characteristic curve of the TiO_2/rGO FET sensor at V_{ds} = 0.5 V. (b) The output characteristic curve of the TiO_2/rGO FET under different V_{gs}. (c) Comparison of the output characteristic curve for the sensors with interdigital electrodes and conventional electrodes. (d) The response-recovery curve of the TiO_2/rGO FET when exposed to 20 ppm SO_2 gas, under the condition of V_{gs} = 0 V and V_{ds} = 2 V (three successive operation cycles in the inset).

acceptor to absorb electrons in the n-type rGO. Electrons in n-type TiO_2 combine with O_2 molecules in the air to generate O_2^-, then SO_2 combines with $O_2^-$to generate electrons, and the generated electrons are re-injected into TiO_2. After about 8 mins, I_{ds} increases slowly and gradually approaches to a maximum state. The sensor is then exposed to air and I_{ds} begins to descend and return to its initial state. Here, I_g and I_a represent the source-drain currents when the TiO_2/rGO FET is exposed to the SO_2 gas and dry air, respectively. Response time refers to the period from the time when the concentration of SO_2 reaches a specific value to that when the TiO_2/rGO FET generates a corresponding current. Recovery time refers to the period from when the current of the sensor return to its initial value after the concentration of SO_2 is zero [3]. The response and recovery times of the sensors are measured as 456 s and 134 s, respectively. When the sensing element is exposed to a specific gas concentration, the change in the resistance or current value is defined as the responsivity [28], with the expression [29]:

$$R = \frac{|I_a - I_g|}{I_g} \times 100\% \quad (1)$$

The value of I_a and the maximum value of I_g are 3.75 mA and 3.885 mA, respectively. Hence, in one working cycle, the maximum responsivity is calculated as 3.47%. The illustration in Fig. 4d shows the response-recovery curve of the TiO_2/rGO FET exposed to 20 ppm SO_2 gas in three consecutive cycles at room temperature. The current of the sensor can return to the baseline after each cycle, indicating a good repeatability.

The response performance of the SO_2 gas sensors proposed in this paper and the results from the literatures are listed and compared in Table 1. Compared with other gas sensors, our sensors have the smallest sensing area and larger responsivity (studies have been shown that the responsivity is proportional to the sensing area and gas concentration), providing a possibility for miniaturized and integrated SO_2 gas sensors.

Fig. 5a shows the responsivity variation of the TiO_2/rGO FET SO_2 gas sensor against the gas concentration from 10 to 80 ppm under the condition of V_{gs} = 0 V and V_{ds} = 0.5 V. With the increase in SO_2 gas concentration, the responsivity value gradually increases, due to the increase in the number of SO_2 gas molecules adsorbed on the surface of the sensor layer. Fig. 5b shows the responsivity variation for various values of gate voltages ranging from −2 to 8 V under V_{ds} = 0.5 V and C = 20 ppm. A minimum responsivity is observed at V_{gs} = 4 V, suggesting that the gate voltage has an influence on the responsivity of SO_2 gas.

Table 1
Response performance of SO_2 gas sensors based on rGO and other materials.

Materials	Temperature	SO_2 gas concentration	Responsivity	Gas sensing area	Ref
SnO_2	220 °C	500 ppm	1.2%	n/a	[21]
rGO	27 °C	5 ppm	3.21%	n/a	[17]
Pt/rGO	120 °C	100 ppm	5%	7.5 × 3.5 mm^2	[16]
rGO/ SnO_2	60 °C	500 ppm	22.6%	n/a	[21]
MOFs TiO_2/ rGO	RT	20 ppm	R_g/R_a = 2.1	1 × 1 cm^2	[24]
TiO_2/rGO	RT	20 ppm	3.47%	130 × 200 μm^2	This work

To explore the influence of source-drain voltage on the response of the TiO_2/rGO FET, the responsivity of the sensor is measured under different source-drain voltages, as shown in Fig. 5c. From Fig. 5c, the responsivity increases from 2.63% to 3.46%, when V_{ds} increase from 0.1 to 2 V. It reveals that the bias has a good regulation on the responsivity. This phenomenon can be explained by the transport capacity of carriers. With the increase in V_{ds}, the transport rate of carriers in the TiO_2/rGO composite sensing film becomes faster, improving both the electrical performance and responsivity of the TiO_2/rGO FET. Furthermore, long-term large bias voltage will increase the temperature of the TiO_2/rGO film and accelerate the adsorption and desorption of SO_2 gas molecules on the surface of the sensing film [30]. Therefore, the response of the sensor can be further improved by applying an appropriate bias voltage. The response-recovery time of the sensor as a function of V_{ds} at V_{gs} = 0 V and C = 20 ppm, as shown in Fig. 5d. The sensor has the highest and lowest response time when V_{ds} are equal to 0.1 and 1 V, respectively. Although the recovery time of the sensor presents an upward trend, the recovery time increases slowly with the increase of V_{ds}.

4. Conclusions

In summary, a novel room temperature SO_2 gas sensor with buried-gate FET and interdigitated electrode structure is proposed, which is

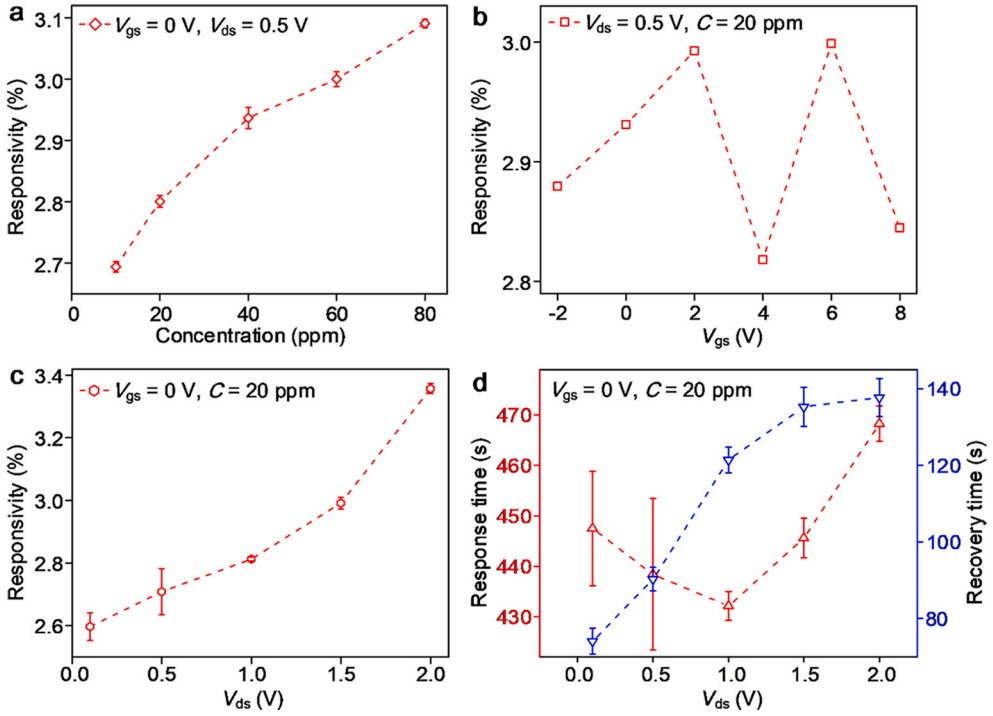

Fig. 5. Response of the TiO_2/rGO FET. (a) The responsivity curve of the sensor as a function of SO_2 concentration under $V_{gs} = 0$ V and $V_{ds} = 0.5$ V. (b) Gate-voltage-dependent responsivity of the sensor under $V_{ds} = 0.5$ V and $C = 20$ ppm. (c) Source-drain-voltage-dependent responsivity of the sensor under $V_{gs} = 0$ V and $C = 20$ ppm. (d) Response-recovery time of the sensor with 20 ppm SO_2 gas under different V_{ds}.

based on TiO_2 nanoparticles and rGO composite gas-sensitive film. The hybrid nanostructures formed by combining rGO with TiO_2 could work at room temperature with high sensitivity. It has been demonstrated that a sensitivity is up to 3.46% with a concentration of 20 ppm under a source-drain voltage of 2 V and a zero gate voltage. The experimental results show that the responsivity and response-recovery time of the sensor are greatly related to the source-drain voltage. Meanwhile, the interdigitated electrode structure could improve the sensing capability. Moreover, the sensor not only has a small sensing area that is easily to be integrated, but also its preparation process is compatible with the traditional MEMS process. The TiO_2/rGO room temperature SO_2 gas sensor with buried-gate FET and interdigitated electrode structure would provide a new idea for the exploration of room temperature SO_2 gas sensor with high sensitivity, miniaturization and easy integration features.

CRediT authorship contribution statement

Simei Zeng: Investigation, Supervision, Visualization, Writing – original draft, Writing – review & editing. **Ying Zhang:** Methodology, Investigation, Resources, Writing – original draft. **Yang Zhang:** Conceptualization, Investigation, Resources. **Yuning Li:** Supervision. **Chenggang Tang:** Supervision, Validation. **Ke Li:** Visualization. **Jingye Sun:** Writing – review & editing. **Tao Deng:** Conceptualization, Methodology, Supervision, Visualization, Writing – review & editing.

Declaration of Competing Interest

The authors declare that they have no known competing financial interests or personal relationships that could have appeared to influence the work reported in this paper.

Acknowledgements

This work was funded by the National Natural Science Foundation of China (No. 61604009), the National Natural Science Foundation of China (No. 61901028) and the Beijing Municipal Natural Science Foundation (No. 4202062).

References

[1] J. Yun, C. Zhu, Q. Wang, et al., Catalytic conversions of atmospheric sulfur dioxide and formation of acid rain over mineral dusts: molecular oxygen as the oxygen source[J], Chemosphere 217 (2019) 18–25.
[2] S.C. Lee, B.W. Hwang, S.J. Lee, et al., A novel tin oxide-based recoverable thick film SO_2 gas sensor promoted with magnesium and vanadium oxides[J], Sensors Actuators B Chem. 160 (1) (2011) 1328–1334.
[3] X. Liu, S. Cheng, H. Liu, et al., A survey on gas sensing technology[J], Sensors 12 (7) (2012) 9635–9665.
[4] D. Zhang, J. Wu, P. Li, et al., Room-temperature SO_2 gas-sensing properties based on a metal-doped MoS_2 nanoflower: an experimental and density functional theory investigation[J], J. Mater. Chem. A 5 (39) (2017) 20666–20677.
[5] X. Chen, X. Wang, J. Huang, et al., Nonmalignant respiratory mortality and long-term exposure to PM10 and SO_2: a 12-year cohort study in northern China[J], Environ. Pollut. 231 (1) (2017) 761–767.
[6] X. Xie, Y. Xia, Research and application of gas sensors: the core of electronic nose [J], Univ. Chem. (2021) 2012045.
[7] A. Marikutsa, M. Rumyantseva, E.A. Konstantinova, et al., The key role of active sites in the development of selective metal oxide sensor materials[J], Sensors 21 (7) (2021) 2554.
[8] Y. Wang, X. Jiang, Y. Xia, A solution-phase, precursor route to polycrystalline SnO_2 nanowires that can be used for gas sensing under ambient conditions[J], J. Am. Chem. Soc. 125 (52) (2003) 16176–16177.
[9] Y.H. Cho, Y.C. Kang, J.H. Lee, Highly selective and sensitive detection of trimethylamine using WO_3 hollow spheres prepared by ultrasonic spray pyrolysis [J], Sensors Actuators B Chem. 176 (2013) 971–977.
[10] Q. Wan, Q.H. Li, Y.J. Chen, et al., Fabrication and ethanol sensing characteristics of ZnO nanowire gas sensors[J], Appl. Phys. Lett. 84 (18) (2004) 3654–3656.
[11] Nisar Jawad, Zareh, et al., TiO_2-based gas sensor: a possible application to SO_2[J], ACS Appl. Mater. Interfaces 5 (17) (2013) 8516–8522.
[12] W. Jin, T. Kai, J. Miao, et al., Graphene for future high-performance gas sensing [M], Springer International Publishing, 2017, pp. 347–363.
[13] S. Pei, H.M. Cheng, The reduction of graphene oxide[J], Carbon 50 (9) (2012) 3210–3228.
[14] L.J. Zhou, X.X. Zhang, W.Y. Zhang, Sulfur dioxide sensing properties of MOF-derived $ZnFe_2O_4$ functionalized with reduced graphene oxide at room temperature [J], Rare Metals 40 (6) (2021) 1604–1613.
[15] P.G. Su, Y.L. Zheng, Room-temperature ppb-level SO_2 gas sensors based on RGO/WO_3 and MWCNTs/WO_3 nanocomposites[J], Anal. Methods 13 (6) (2021) 782–788.

[16] D. Chen, J. Tang, X. Zhang, et al., Detecting decompositions of sulfur hexafluoride using reduced graphene oxide decorated with Pt nanoparticles[J], J. Phys. D. Appl. Phys. 51 (18) (2018), 185304.
[17] R. Kumar, A. Kaur, Chemiresistive gas sensors based on thermally reduced graphene oxide for sensing sulphur dioxide at room temperature[J], Diam. Relat. Mater. 109 (2020), 108039.
[18] N. Minh Triet, L. Thai Duy, B.U. Hwang, et al., High-performance Schottky diode gas sensor based on the heterojunction of three-dimensional nanohybrids of reduced graphene oxide-vertical ZnO nanorods on an AlGaN/GaN layer[J], ACS Appl. Mater. Interfaces 9 (36) (2017) 30722–30732.
[19] D.B. Moon, A. Bag, H.B. Lee, et al., A stretchable, room-temperature operable, chemiresistive gas sensor using nanohybrids of reduced graphene oxide and zinc oxide nanorods[J], Sensors Actuators B Chem. 345 (2021) 130373.
[20] A. Chen, R. Liu, X. Peng, et al., 2D hybrid nanomaterials for selective detection of NO_2 and SO_2 using "light on and off" strategy[J], ACS Appl. Mater. Interfaces 9 (42) (2017) 37191–37200.
[21] P. Tyagi, A. Sharma, M. Tomar, et al., A comparative study of rGO-SnO_2 and MWCNT-SnO_2 nanocomposites based SO_2 gas sensors[J], Sensors Actuators B Chem. 248 (2017) 980–986.
[22] W. Li, J. Guo, L. Cai, et al., UV light irradiation enhanced gas sensor selectivity of NO_2 and SO_2 using rGO functionalized with hollow SnO_2 nanofibers[J], Sensors Actuators B Chem. 290 (2019) 443–452.
[23] D. Zhang, J. Liu, C. Jiang, et al., High-performance sulfur dioxide sensing properties of layer-by-layer self-assembled titania-modified graphene hybrid nanocomposite[J], Sensors Actuators B Chem. 245 (2017) 560–567.
[24] D. Zhang, D. Wu, X. Zong, et al., Enhanced SO_2 gas sensing properties of metal organic frameworks-derived titanium dioxide/reduced graphene oxide nanostructure[J], J. Mater. Sci. Mater. Electron. 30 (12) (2019) 11070–11078.
[25] R. Kumar, D.K. Avasthi, A. Kaur, Fabrication of chemiresistive gas sensors based on multistep reduced graphene oxide for low parts per million monitoring of sulfur dioxide at room temperature[J], Sensors Actuators B Chem. 242 (2017) 461–468.
[26] Y. Yanagisawa, Oxygen exchange between SO_2 adsorbate and TiO_2 surfaces[J], Appl. Surf. Sci. 115 (4) (1997) 377–380.
[27] J. Tamaki, T. Hashishin, Y. Uno, et al., Ultrahigh-sensitive WO_3 nanosensor with interdigitated au nano-electrode for NO_2 detection[J], Sensors Actuators B Chem. 132 (1) (2008) 234–238.
[28] J. Huang, Q. Wan, Gas sensors based on semiconducting metal oxide one-dimensional nanostructures[J], Sensors 9 (12) (2009) 9903–9924.
[29] S.J. Patil, A.V. Patil, C.G. Dighavkar, et al., Semiconductor metal oxide compounds based gas sensors: a literature review[J], Front. Mater. Sci. 9 (1) (2015) 14–37.
[30] S. Xu, F. Sun, Z. Pan, et al., Reduced graphene oxide-based ordered macroporous films on a curved surface: general fabrication and application in gas sensors[J], ACS Appl. Mater. Interfaces 8 (5) (2016) 3428–3437.